*Am J Physiol Cell Physiol* 315: C623–C635, 2018.
First published July 25, 2018; doi:10.1152/ajpcell.00157.2018.

**RESEARCH ARTICLE**

# Alterations at $Arg^{76}$ of human connexin 46, a residue associated with cataract formation, cause loss of gap junction formation but preserve hemichannel function

**Charles K. Abrams,[1,2] Alejandro Peinado,[1] Rola Mahmoud,[2] Matan Bocarsly,[2] Han Zhang,[3] Paul Chang,[3] Wesley M. Botello-Smith,[3] Mona M. Freidin,[1,2] and Yun Luo[3]**

[1]*Department of Neurology and Rehabilitation, University of Illinois at Chicago College of Medicine, Chicago, Illinois;* [2]*Department of Neurology State University of New York Downstate Medical Center, Brooklyn New York; and* [3]*Department of Pharmaceutical Sciences, College of Pharmacy, Western University of Health Sciences, Pomona, California*

Submitted 24 April 2018; accepted in final form 23 July 2018

**Abrams CK, Peinado A, Mahmoud R, Bocarsly M, Zhang H, Chang P, Botello-Smith WM, Freidin MM, Luo Y.** Alterations at $Arg^{76}$ of human connexin 46, a residue associated with cataract formation, cause loss of gap junction formation but preserve hemichannel function. *Am J Physiol Cell Physiol* 315: C623–C635, 2018. First published July 25, 2018; doi:10.1152/ajpcell.00157.2018.—The connexins are members of a family of integral membrane proteins that form gap junction channels between apposed cells and/or hemichannels across the plasma membranes. The importance of the arginine at position 76 ($Arg^{76}$) in the structure and/or function of connexin 46 (Cx46) is highlighted by its conservation across the entire connexin family and the occurrence of pathogenic mutations at this (or the corresponding homologous) residue in a number of human diseases. Two mutations at $Arg^{76}$ in Cx46 are associated with cataracts in humans, highlighting the importance of this residue. We examined the expression levels and macroscopic and single-channel properties of human Cx46 and compared them with those for two pathogenic mutants, namely R76H and R76G. To gain further insight into the role of charge at this position, we generated two additional nonnaturally occurring mutants, R76K (charge conserving) and R76E (charge inverting). We found that, when expressed exogenously in Neuro2a cells, all four mutants formed membrane hemichannels, inducing membrane permeability at levels comparable to those recorded in cells expressing the wild-type Cx46. In contrast, the number of gap-junction plaques and the magnitude of junctional coupling were reduced by all four mutations. To gain further insight into the role of $Arg^{76}$ in the function of Cx46, we performed homology modeling of Cx46 and in silico mutagenesis of $Arg^{76}$ to Gly, His, or Glu. Our studies suggest that the loss of interprotomeric interactions has a significant effect on the extracellular domain conformation and dynamics, thus affecting the hemichannel docking required for formation of cell-cell channels.

cataract; connexin; gap junction; hemichannel

## INTRODUCTION

The human connexins are members of a family of integral membrane proteins that form cell-cell channels between apposed cells [gap junction (GJ) channels] and/or hemichannels across the plasma membranes. In the past decade, however, other roles are being described for connexins. GJs may be part of a larger complex that contains other junctional elements. Several connexins, including connexin 43 (Cx43) and Cx47, have PDZ-binding domains on their COOH termini, and bind to ZO-1, one of the defining members of the PDZ family (17, 22, 28, 29, 35, 43, 53). Other data suggest that connexins may have roles in regulation of cell growth (13, 15, 33, 37, 45) and resistance to both apoptotic and necrotic cell death (30, 36) that are independent of formation of functional GJ channels.

There are at least 21 human members of the connexin family (52) and at least two of these, Cx46 (41) and Cx50 (61), are expressed in mature human lens fiber cells. In the lens, Cx46 and Cx50 are critical for lens transparency. Because the lens is an avascular tissue, these connexins are thought to serve as an internal circulatory system (5). Mutations in each of these two connexins may disrupt this function, leading to cataract formation.

The importance of the arginine at position 76 ($Arg^{76}$) in the structure and/or function of human Cx46 wild-type (Cx46) is highlighted by its conservation across the entire connexin family and by the occurrence of pathogenic mutations at this (or the corresponding homologous) residue in a number of human diseases. These include Cx26-associated deafness (48), Cx32-associated neuropathy and central nervous system dysfunction (55), Cx43-associated occulodentatodigital dysplasia (42), and Cx46-associated cataracts (8). [See Supplementary Table I of Abrams et al. (4) for additional references.] Thus, a better understanding of the effects of mutations of this codon in these connexins may have relevance to pathogenesis of a number of different human diseases.

Previous studies have examined the effects of mutation at $Arg^{76}$ in Cx43 (or the homologous residue at position $Arg^{75}$ in Cx32 and Cx26). Homology modeling of Cx32 (4) based on the crystal structure of Cx26 (32), and a refined structure of Cx26 determined utilizing molecular dynamics (MD) simulations (25), predict that in Cx32 $Arg^{75}$ participates in an electrostatic cluster of residues, with intrasubunit interactions with $Glu^{47}$ and intersubunit interactions with $Glu^{186}$, while $Glu^{47}$ shows intersubunit interactions with $Arg^{183}$.

Two mutations (8, 12) at the homologous residue in Cx46 ($Arg^{76}$) are associated with cataracts in humans, highlighting the importance of this residue in the function of human Cx46. In this communication, we examined the expression levels and

Address for reprint requests and other correspondence: C. K. Abrams, Dept. of Neurology and Rehabilitation, Univ. of Illinois at Chicago College of Medicine, 912 Wood St., Chicago, IL 60612 (e-mail: cabrams1@uic.edu).

  

macroscopic and single-channel properties of human Cx46 and compared them with those for two pathogenic mutants, namely R76H (8) and R76G (12). To gain further insight into the role of charge at this position, we examined the properties of two additional non-disease-causing mutants, R76K and R76E.

We found that, when expressed exogenously in Neuro2a cells, all four mutations efficiently form membrane hemichannels, inducing membrane permeabilities at levels similar to those for wild-type (WT). On the other hand, junctional coupling is reduced for R76E, R76G, and R76H and eliminated for R76K; in addition, there was a commensurate reduction in gap junction plaques for each of these mutants. We further show that, unlike what was seen for Cx32 (4), charge change at this position (R76E) did not lead to dramatic alteration in conductance-voltage relations, and the presence of a positive charge at this position was not sufficient to preserve the ability to form cell-cell channels. However, our studies suggest that the loss of the $Arg^{76}$ may play a role in the ability of the Cx46 hemichannel to dock with an apposed hemichannel to form a cell-cell channel. Thus, it is likely that the loss of interprotomeric electrostatic interactions has a significant effect on the extracelluar domain conformation and dynamics, thus affecting the hemichannel docking. Our correlation analysis using the last 20-nS trajectories indeed show a strong correlation in the dynamic motion between $Arg^{76}$ and residues at the docking interface (residues 170–196). This observation, along with experimental results, supports our hypothesis that R76 mutation may allosterically affect junctional docking.

## METHODS

*Production of mutants.* Mutants were introduced into a construct containing the human *GJA3* coding region cloned into pIRES2-green fluorescent protein (EGFP; Clontech, Mountain View, CA), using the QuikChange II XL Site-Directed Mutagenesis Kit (Stratagene, La Jolla, CA). The entire coding region of each construct was confirmed by sequencing. (Mutations are referred to using *s*ingle-letter codes. WT residues are referred to as "three-letter code codon number".)

Neuro2a cells were obtained directly from ATCC (Manassas, VA). These cells, authenticated as to identity and certified as mycoplasma free, were used for all experiments. Only cells from passages 9 through 20 were used.

*Immunofluorescent labeling.* Neuro2a cells were transiently transfected with 500 ng of WT or mutant Cx46 constructs by using LTX and Plus Reagent (Life Technologies, Grand Island, NY) per the manufacturer's instructions. The cultures were incubated for 24 h before being processed for immunofluorescence labeling, immunelabeled for Cx46 using mouse anti Cx46 and Alexa 594 goat anti-mouse secondary antibodies, and counterstained with 4′,6-diamidino-2-phenylindole (DAPI), as previously described (39). Slides were imaged using an Olympus FV1000 confocal microscope with a ×60 oil immersion lens (numerical aperture 1.4) with identical photomultiplier tube, pinhole aperture, and laser power settings. Images were produced by taking the maximum intensity projection of six adjacent optical sections from a single Z-stack. Individual images for display were montaged and adjusted for brightness and contrast in Adobe Photoshop (Mountain View, CA).

*Immunofluorescence-based quantitation of connexin expression and Triton X insoluble fraction.* For each experiment, Neuro2a cells were transfected with 500 ng of DNA per well with LTX and Plus Reagent (Life Technologies, Grand Island, NY) in single wells of a 12-well plate for each mutant. Twelve hours later, cells were plated onto four coverslips (two for treatment and two as controls). Twenty-four hours later, cells were washed twice with Hank's balanced salt solution (HBSS) + Complete Mini Protease Inhibitor Cocktail (Roche) in HBSS while on ice, followed by a 30-min treatment with protease inhibitors +1% Triton X-100 (Sigma-Aldrich, St. Louis, MO) in 10 ml of HBSS or protease inhibitors in HBSS alone. Cells were then washed once with PBS, fixed with 4% PFA for 15 min at room temperature, washed and stored in PBS-Tween 0.05% at 4°C, and immunolabeled for Cx46 as above. Slides were imaged at ×20 (NA 0.5) using an Olympus Bx61 microscope outfitted for epifluorescence in conjunction with a Retiga digital CCD camera using a uniform exposure time (Q-Imaging, Surrey, BC, Canada). Regions were selected using the DAPI signal to select nonoverlapping areas with similar high cellular density, without looking at Cx46 labeling. For control coverslips (−Triton), four regions were photographed per coverslip, whereas for Triton-treated coverslips 4–7 regions were selected (densities were somewhat lower with Triton treatment) to achieve similar numbers of total nuclei per condition. For each image, total integrated fluorescence was normalized to total number of DAPI-positive nuclei to obtain mean integrated fluorescence per cell (MIF/cell). Average MIF/cell for each pair of coverslips constituting a single experiment was determined for untreated (Triton-negative) WT and Cx46 mutants. Then MIF/cell for each image from the Triton-treated cells was normalized to average MIF/cell for the untreated coverslips from that experiment, and the normalized values were averaged to produce an average MIF/cell normalized to the overall level of expression for that experiment. The results of the individual experiments for each mutant or WT were then averaged and compared.

*Dye uptake for analysis of hemichannel function.* Neuro2a cells previously transfected with either EGFP-expressing vector alone or vector expressing WT or mutant Cx46 along with EGFP under an IRES element, were exposed for 2 h (at 37°C) to culture medium containing DAPI (700 nM), a small (molecular weight 277) fluorescent molecule that can permeate through most connexin channels. The dye permeates cells expressing plasma membrane hemichannels and increases its fluorescence quantum yield upon binding to nuclear DNA, providing a sensitive assay for the presence of functional hemichannels on cells. Hemichannel block was achieved by using either 1 mM octanol or 200 μM lanthanum ($LaCl_3$) during the DAPI incubation. All dye uptake experiments involving blockade of WT hemichannels with $LaCl_3$ (and the parallel controls without $LaCl_3$) were done in Tyrode bath solution (in mM): 150 NaCl, 4 KCl, 1 $MgCl_2$, 2 $CaCl_2$, 5 dextrose, 2 pyruvate, and 10 HEPES, pH 7.4. Utilization of Tyrode medium avoided absorption of $La^{3+}$ by serum proteins in the cell culture medium.

Fields of live cells were viewed at ×10 magnification using a Nikon fixed-stage (E600FN) epifluorescence microscope equipped for DAPI (350 em/480 ex) and EGFP (470 em/535 ex) fluorescence, and a ×0.5 trinocular adapter. IPLab Windows software (Scanalytics) and a SVGA Sensicam CCD camera (Cooke, Tonawanda, NY) were used to acquire separate DAPI and EGFP images for each field of cells. Exposure to fluorescent light and the potential for photobleaching were minimized by acquiring single images for each chromophore (exposure: 500 ms; pixel binning: 2 × 2) which were subsequently analyzed offline. Fluorescence intensities were determined by manually placing circular regions of interest (ROIs; diameter: 10 binned pixels) over the nucleus of each cell on the DAPI image. The mean DAPI pixel intensity for each ROI was recorded and saved before transferring the entire set of ROIs from the DAPI image to the EGFP image to likewise record the mean pixel intensity at the same locations on the green channel image. The paired EGFP and DAPI values for each cell within a field were used to derive a measure of the statistical correlation between DAPI and EGFP fluorescence intensities using GraphPad Prism 5.04 for Windows. We report the average slopes of the correlations for each of several fields of cells obtained from each of 3–5 independent experiments.

*Dual whole cell recordings.* pIRES2-EGFP vectors containing DNA encoding human wild-type Cx46 (Cx46WT) or mutants were

transiently transfected as above into confluent Neuro2a cells. Homotypic cell pairs were prepared by replating 1 day following transfection. For heterotypic cell pairs, transfected cells were washed, and cells expressing a pIRES2-EGFP construct expressing mutant Cx46 were mixed with cells expressing a pIRES2-DsRed construct expressing wild-type Cx46, in a 1:1 ratio. Coupling was assessed by dual whole cell patch clamping of cell pairs 6–48 h after replating, as previously described (4). Only cells clearly expressing the appropriate fluorescent proteins (thus indicating that they were transfected) were used for recording. Recording solutions used were as follows (in mM): pipette solution, 145 CsCl, 5 EGTA, 1.4 $CaCl_2$, and 5.0 HEPES, pH 7.2; bath solution, Tyrode as above. Heterotypic pairings between cells are shown as "connexin expressed in cell 2/connexin expressed in cell 1". Normalized junctional conductance-junctional voltage ($G_j$-$V_j$) relations were determined from isolated pairs by measuring junctional current ($I_j$) elicited in cell 2 in response to 5-s junctional voltage pulses (from −100 mV to +100 mV in 20-mV increments) applied to cell 1, and applying Ohm's law. For the $G_j$-$V_j$ plot, steady-state conductance levels were estimated by fitting current traces to a sum of exponentials and using the conductance level at $t = \infty$. Baseline ($V_j = 0$) junctional conductances were similarly determined by measuring instantaneous $I_j$ responses to voltage steps from $V_j = 0$ to +40 mV and to −40 mV and using the average of the two measurements. Cytoplasmic bridges were excluded by demonstrating sensitivity of junctional conductance to application of octanol-containing bath solution (data not shown). For the $G_j$-$V_j$ plot, data were imported into Origin (Originlab, Northampton, CA), and fitted to a "double Boltzmann" equation of the form

$$G_{ss}(V) = \left[G_{min1} + \left(G_{max1} - G_{min1}\right)/\left(1 + e^{[K1(V-V01)]}\right)\right] * \left[G_{min2} + \left(G_{max2} - G_{min2}\right)/\left(1 + e^{[K2(V-V02)]}\right)\right]$$

where $G_{ss}$ is the steady-state junctional conductance normalized to $V_j = 0$, $G_{max1}$ and $G_{max2}$ are the maximal and $G_{min1}$ and $G_{min2\ are}$ the minimal normalized conductances for the limb reflecting the normalized residual conductances for the negative or positive limbs, and $V_{01}$ and $V_{02}$ are the voltages at which the conductance for the negative or positive limb is 1/2 the difference between $G_{min}$ and $G$ for that limb. $K_1$ and $K_2$ are parameters that reflect the slope of the negative or positive limb of the $G_j$-$V_j$ plot and are a measure of voltage sensitivity. The general use of a double Boltzmann requires a number of assumptions. However, in cases where only one limb is changing at any given voltage and the other limb has a value of 1 at those voltages, such as is the case here, use of the double Boltzmann is mathematically equivalent to fitting limbs individually. See Abrams et al. (2) for further discussion.

*Statistics.* All statistical tests were performed in GraphPad Prism. For Triton X extractions and DAPI uptake experiments, results were compared using ANOVA with Holmes-Sidak post test. For dual whole cell patch-clamp assays, junctional conductance values were compared using the Kruskal-Wallis test with Dunn's post test.

*Homology modeling and in silico mutagenesis.* The previously MD-equilibrated Cx26 model (25, 27, 31) was used as a structure template to build the homology model of human Cx46 by using the MOE homology modeling tool (8a). The CT domains of Cx46 are significantly larger than those of the Cx26; thus, only the residues 2–237 were modeled. All of the equilibrated models are provided in PDB format in the Supplemental Material (Supplemental Material for this article is available online at the Journal website). CHARMM-GUI (20) was used to construct the human Cx46 systems, including the membrane and solvent. The system was initially neutralized with $Cl^-$, followed by addition of $K^+$ and $Cl^-$ to yield a concentration of 0.1 M KCl. The Cx46 hexamer was solvated in a fully hydrated 1-palmitoyl-2-oleoylphosphatidylcholine (POPC) bilayer with a 15-Å layer of explicit water above and below the bilayer. The total number of atoms was 238,688. In the simulations, the channel was aligned along the z-axis/membrane normal. CHARMM parameter sets were used throughout, including the CHARMM36 parameters for the protein (6), lipids (23), and ions, and TIP3P for water (21). All simulations were performed using the PMEMD module of the AMBER16 package with support for MPI multiprocess control and GPU acceleration code. Orthorhombic periodic boundary conditions were used for all simulations in the isobaric-isothermal (NPT) ensemble using Langevin thermostat and Monte-Carlo barostat. The pressure and temperature were maintained at 1 atm and 303.15 K. Long-range electrostatic interactions were treated using the particle mesh Ewald (PME) method. A smoothing function was applied to van der Waals forces between 10 and 12 Å. The dynamics were propagated using Langevin dynamics with Langevin damping coefficient of 1 $ps^{-1}$ and a time step of 2 fs. The SHAKE algorithm was applied to all hydrogen atoms. The pairwise interaction decomposition was calculated using the LIE method in AMBER16. Salt bridges were predicted using ESBRI (10) with a cutoff distance of 4.0 Å. Correlation maps were computed using the program CARMA (18) and plotted using R script.

## RESULTS

*Mutant forms of Cx46 show reduced functional expression in Neuro2a cells.* To evaluate the properties of Cx46 and the four mutants at $Arg^{76}$, we expressed each in Neuro2a cells and quantitated the degree of coupling between pairs of transfected cells, identified by the presence of EGFP or DsRed fluorescence. (See METHODS for details). As shown in Table 1, a majority of examined wild-type expressing cells were coupled, albeit to varying degrees. Both degree of coupling and percentage of coupled cells was reduced compared with what we typically obtain with other wild-type connexins (3, 39). This relative inefficiency of coupling for human Cx46WT is similar to what has been reported by other investigators (56). However, relative to the wild-type, all four mutants examined

Table 1. *Function coupling of Neuro2a cells expressing WT or mutant Cx46 in the homotypic or heterotypic configuration*

| Pairing Configuration | *n* (pairs) | Not Coupled | Median, nS | Mean, nS | SD, nS | SE, nS | *P* vs. WT | *P* vs. IE |
|---|---|---|---|---|---|---|---|---|
| Cx46WT/Cx46WT | 55 | 18 | 419 | 1,809 | 3,110 | 419.4 | | * |
| R76E/R76E | 16 | 13 | 0 | 44.19 | 152.8 | 38.2 | ‡ | NS |
| R76G/R76G | 22 | 17 | 0 | 561.7 | 1407 | 299.9 | ‡ | NS |
| R76H/R76H | 24 | 16 | 0 | 197.8 | 488.8 | 99.77 | † | NS |
| R76K/R76K | 12 | 12 | 0 | 0 | 0 | 0 | ‡ | NS |
| IE/IE | 15 | 7 | 44 | 73.27 | 120.3 | 31.07 | * | NS |
| R76E/46WT | 12 | 8 | 0 | 63.58 | 140.1 | 40.44 | * | NS |
| R76G/46WT | 16 | 12 | 0 | 61.88 | 117.5 | 29.39 | † | NS |
| R76H/46WT | 12 | 9 | 0 | 246.7 | 559.2 | 161.4 | * | NS |
| R76K/46WT | 7 | 7 | 0 | 0 | 0 | 0 | † | NS |

Cx46, connexin 46; *n*, no. of cell pairs; WT, wild-type; SD, standard deviation; SE, standard error; nS, nanoSiemen; IE, IRES2-EGFP (empty vector). Significance determined using Kruskal-Wallace with Dunn's post test: *$P < 0.05$; †$P < 0.01$; ‡$P < 0.005$.

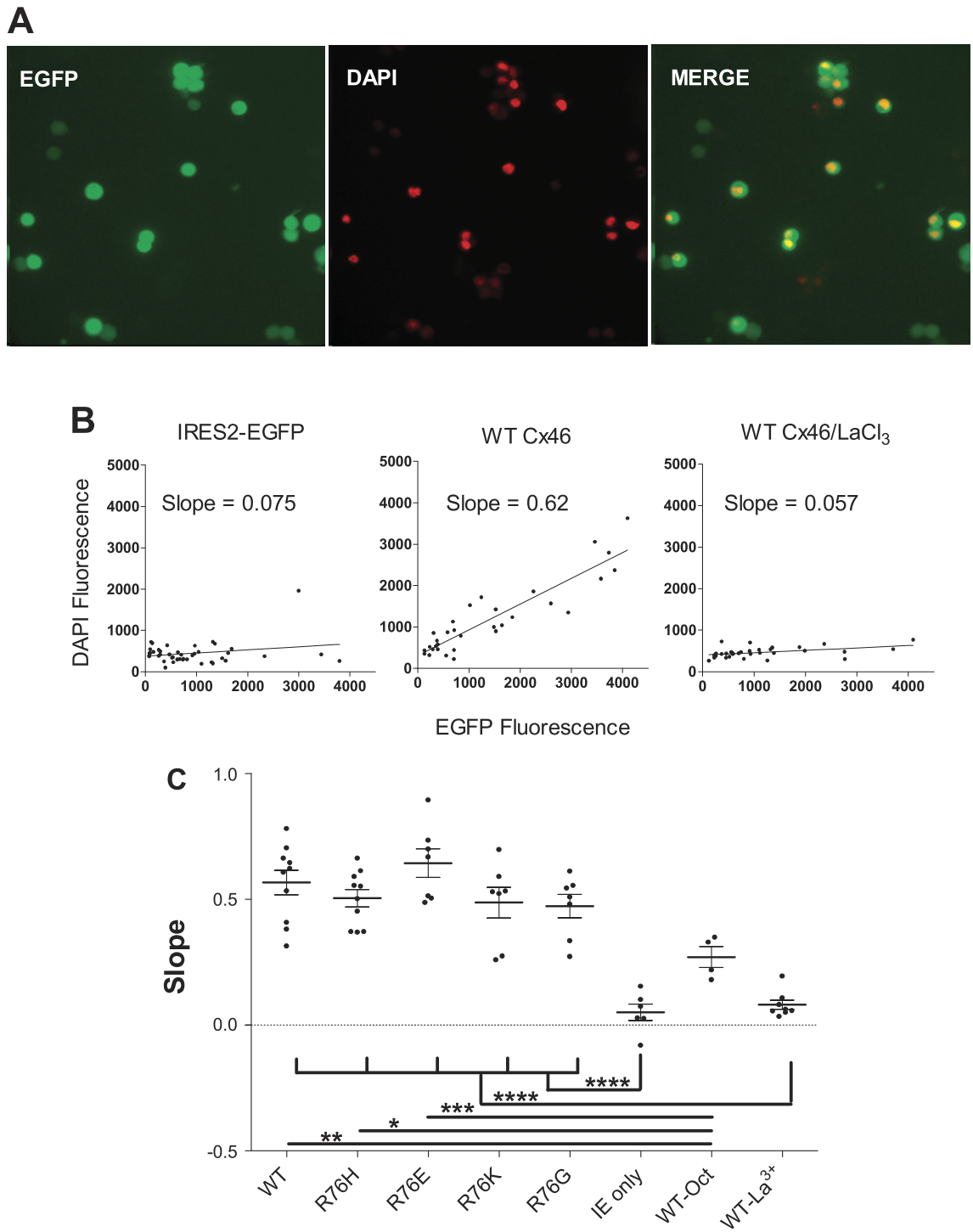


Fig. 1. Neuro2A cells expressing wild-type (WT) or mutant forms of connexin (Cx)46 mediate similar levels of uptake of DAPI, a fluorescent dye known to permeate through Cx46 hemichannels. *A*: representative images showing WT Cx46-expressing green [enhanced green fluorescent protein (EGFP)-expressing] cells and red pseudocolored nuclei indicating DAPI uptake after 2 h of incubation in dye-containing medium (as described in METHODS). Because transcription of connexin and EGFP are well correlated, we used the latter as a reliable proxy for the level of Cx46 expression in each cell. *B*: correlation between EGFP fluorescence and DAPI fluorescence for cells that were transfected with empty vector [IRES2-EGFP (IE)], WT Cx46, or WT Cx46 and incubated with a Cx46 hemichannel blocker during the DAPI incubation (WT Cx46/$LaCl_3$). In these plots, each data point is one cell. The slope of the linear regression is a measure of the effect that Cx46 hemichannel expression has on dye uptake, provided hemichannels are not blocked. *C*: slope data for all experiments involving cells expressing empty vector (IE), the four mutants (R76H, R76E, R76G, R76K), and the WT Cx46 in the absence or presence of a hemichannel blockers octanol (WT-oct) or $LaCl_3$ (WT-$La^{3+}$). Each data point represents the slope of the EGFP-DAPI correlation derived from all cells in a single experiment. DAPI uptake was positively correlated with EGFP fluorescence intensity in WT and all four mutant-expressing cells but not in cells transfected with the empty vector or in WT-expressing cells subjected to $LaCl_3$ (or to a lesser extent) octanol treatments to block hemichannels. $^*P < 0.05$, $^{**}P < 0.01$, $^{***}P < 0.001$, $^{****}P < 0.0001$; ANOVA with Holm-Sidak post test. No statistically significant difference was found between the WT and any of the mutants.

Table 2. *Mean integrated fluorescence per expressing cell*

| Variant | *n* | Mean Integrated Fluorescence per Cell × $10^5$ | SD × $10^5$ | SE × $10^5$ |
|---|---|---|---|---|
| Cx46WT | 4 | 4.9 | 3.4 | 1.7 |
| R76E | 4 | 3.7 | 0.7 | 0.4 |
| R76G | 4 | 4.9 | 1.8 | 0.9 |
| R76H | 3 | 5.3 | 3.8 | 2.2 |
| R76K | 4 | 5.0 | 2.5 | 1.3 |

Cx46, connexin 46; SD, standard deviation; SE, standard error; WT, wild-type.

produced significantly lower levels of junctional coupling than did wild-type both when paired homotypically and when paired heterotypically with Cx46WT. (Table 1).

*Mutant forms of Cx46 produce functional hemichannels with an efficiency similar to that of WT.* To further assess functional expression, we examined the ability of Cx46WT and the four mutants to produce functional hemichannels. Our transfections utilize a bicistronic vector, leading to expression of mRNA containing the message for both Cx46 and EGFP in a 1:1 ratio. Thus, for a given cell, the level of EGFP protein expression (and fluorescence) correlates with the amount of Cx46 protein (1). The slope of the linear regression line for the relationship between EGFP intensity and DAPI uptake is a measure of the effect that Cx46 hemichannel expression has on dye uptake, assuming hemichannels are not blocked. As shown in Fig. 1, when expressed in Neuro2a cells and bathed in a solution containing 700 nM DAPI, each of these mutants allowed a degree of dye uptake similar to that of WT Cx46, as measured by the average slopes of the DAPI intensity as a function of EGFP intensity. As control experiments, we used cells transfected with EGFP alone or cells transfected with WT Cx46 and EGFP that were treated with $La^{3+}$, a blocker of Cx46 hemichannels, or with octanol. In these controls, the slope of the line for the relationship between EGFP intensity and DAPI uptake is close to zero, consistent with DAPI requiring functional connexin hemichannels to gain access to the cell interior. Our quantitative analysis of immunofluorescence labeling also showed that the WT and the four mutants expressed at similar levels (see Table 2 for quantitation of immunolabeling). Together, these findings suggest that Cx46 protein expression and membrane insertion of functional channels were similar for the wild-type and the four mutants.

*Mutant forms of Cx46 fail to efficiently form gap junction plaques.* A possible explanation for reduced levels of junctional coupling in the cells expressing mutant forms of Cx46 compared with wild-type would be failure to efficiently form junctional plaques. We therefore expressed the WT and four mutant forms of Cx46 exogenously in Neuro2a cells to evaluate their subcellular localization by immunolabeling. Confocal microscopy images of Neuro2a cells that have been transiently transfected to express one of the indicated mutations, empty vector (CTRL), or wild-type Cx46 are shown in Fig. 2. The cells, which were immunolabeled for Cx46 (red) and counterlabeled with DAPI (blue) to label nuclei, showed qualitatively similar levels of Cx46 immunoreactivity in all four cases. As noted above, our quantitative analysis also showed that overall expression of the WT and the four mutants was similar (see Table 2 for quantitation of total integrated fluorescence for Cx46 and mutants). For WT, many apposed cells expressing Cx46 showed intense areas of labeling between them, likely representing gap junction plaques (arrow in Fig. 2*A*.) R76H (plaque not shown) and R76G (arrow in Fig. 2*C*) also rarely showed areas of intercellular labeling. No clear labeling at areas of cell-cell contact was seen for either R76E or R76K mutants. These qualitative findings suggested that only Cx46WT efficiently formed gap junction plaques. To evaluate this in a more quantitative way, we examined whether there were differences in the relative amounts of protein incorporated into gap junction plaques among cells expressing Cx46 or the four mutants. Connexins organized into intercellular plaques are insoluble in Triton X (38, 46, 59), whereas monomers and hexameric hemichannels are soluble. As shown in Fig. 3, nearly 50% of the total normalized Triton-resistant Cx46 immunoreactive material per cell remains after Triton X extraction in cells expressing Cx46WT; in contrast, less than 10% of total Cx46 reactive immunofluorescence is Triton resistant in cells expressing any one of the four Cx46 mutants. This represents a statistically significant reduction for all four mutants compared with wild-type Cx46.

*Properties of cell-cell channels formed by wild-type and mutant Cx46.* We next examined the properties of the wild-type channel, which has not been previously studied in mammalian cells. While the rat Cx46 has been studied (19), the

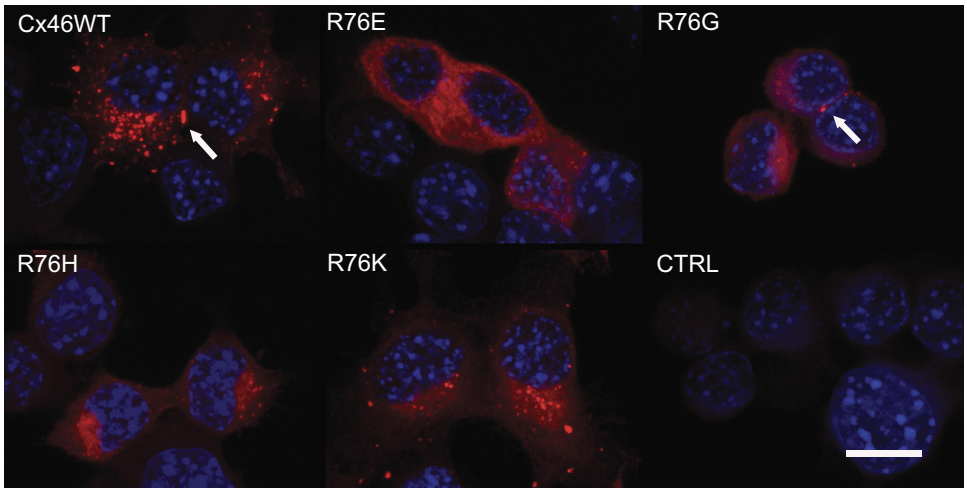


Fig. 2. Connexin expression and plaque formation in Neuro2a cells transfected with wild-type (WT) and mutant Cx46. These are confocal images of Neuro2a cells that have been transiently transfected to express one of the indicated mutations as well as empty vector (CTRL) and WT Cx46. Cells were immunolabeled for Cx46 (red) and counterlabeled with DAPI (blue) to label nuclei. Plaques are shown by arrows. Two of the mutants never displayed gap junction plaques large enough to be resolved, whereas WT showed many, and mutants R76G and R76H showed them extremely rarely. Scale bar, 10 μm.

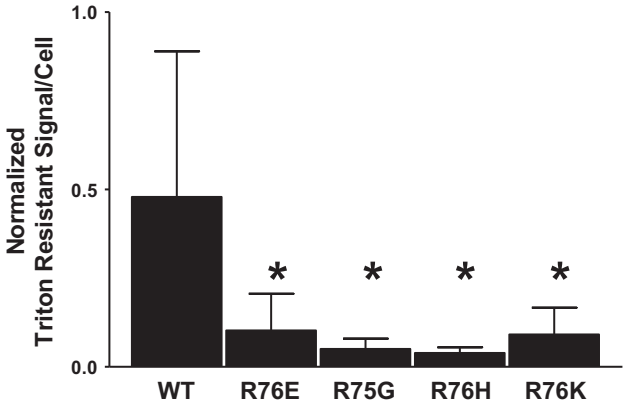


Fig. 3. Normalized Triton X-resistant signal. For each experiment, Triton X-resistant signal per cell was determined for four to seven images and normalized to the total signal per cell from a nontreated sister coverslip from the same transfection to determine the normalized Triton-resistant signal/cell. Values for each experiment and genotype were averaged and displayed as mean ± SD; $n = 4$ for all genotypes, except R76H, where $n = 3$. As shown, all four mutants (R76H, R76E, R76G, R76K) show significantly less normalized Triton-resistant signal than does the wild-type (WT). *$P < 0.05$, ANOVA with Holm-Sidak post test.

primary amino acid sequence of rat Cx46 differs from that of the human sequence by ~30% (69% identity by BLAST; https://blast.ncbi.nlm.nih.gov/Blast.cgi), raising the possibility that some properties may differ. As shown in Fig. 4, the steady-state conductance-voltage relations for Cx46WT shows a bell shape with closure at voltages with absolute values greater than 20 mV and a residual conductance at large positive or negative Vj ~10% of the conductance at $V_j = 0$ mV. These findings differ only minimally from those seen for rat Cx46 (19); furthermore, the predominant single-channel conductance of the human Cx46WT channel calculated from current traces such as those shown in Fig. 5*A* is ~140 pS in 145 mM CsCl, although in a small number of cases larger openings were seen ranging to ~180 pS. Our predominant open-channel conductance is very similar to that noted by some investigators for the rat Cx46 channel (19, 57), although another group reported that the fully open channel formed by rat Cx46 had a unitary conductance of 213 pS in 120 mM KCl (50).

Because of the small number of coupled cells and the very low levels of coupling seen for the four mutants evaluated, we were unable to generate macroscopic conductance voltage relations for any of these. However, we were able to identify unitary conductance transitions recorded from poorly coupled cell pairs for both R76E and R76H in both the homotypic and heterotypic configurations and for R76G in the heterotypic configuration only. The R76K mutant never produced functional coupling in any configuration. The conductance of the fully open R76E mutant calculated from traces such as that shown in Fig. 5*B* was ~110 pS, whereas the conductance of the R76H mutant channel, calculated from current traces such as that shown in Fig. 5*C*, was ~250 pS. (Note that R76E-induced coupling was extremely rare.) Of particular note, and as shown in Fig. 5, *B* and *C*, both the R76E and R76H channels appear to have voltage sensitivities consistent with a high open probability of active channels at small $V_j$. (These findings, however, do not speak to the issue of the efficiency with which a channel becomes active.) We also recorded from poorly coupled cell pairs expressing R76H, R76E, and R76G mutants paired heterotopically with Cx46. As shown in Fig. 6, *A, C,* and *E*, none of the three heterotypic channels showed substantial open channel rectification. Figure 6, *B, D,* and *F*, demonstrate that there was no notable asymmetry of gating. The Cx46WT/R76E channel had a single-channel conductance of ~125 pS, whereas the Cx46WT/R76G channel had a single-channel conductance of ~140–150 pS. For the Cx46WT/R76H pairing, we were unable to obtain a recording with only a single active channel. However, the predominant transition sizes were between 180 and 200 pS, consistent with the higher conductance seen for the homotypic R76H channel.

*Homology modeling and in silico mutagenesis highlight the importance of Arg$^{76}$ in the structure of Cx46.* To gain further insight into the effects of mutation of Arg$^{76}$ on the structure of Cx46, we performed homology modeling of the Cx46 hemichannel by utilizing the previously equilibrated crystal structure of the open channel of Cx26 (25) in conjunction with in silico mutagenesis of the Arg$^{76}$. The wild-type, R76G, R76H, and R76E mutations were each simulated in membrane and solvent environment for 50 ns. The R76K mutant never produced functional coupling, and thus is not considered further in this analysis. In the equilibrated model of Cx26, Arg$^{75}$ (the residue homologous to Arg$^{76}$ in Cx46) forms part of a large inter- and intrasubunit network of ionic interactions that links all six protomers and stabilizes the open state of the channel

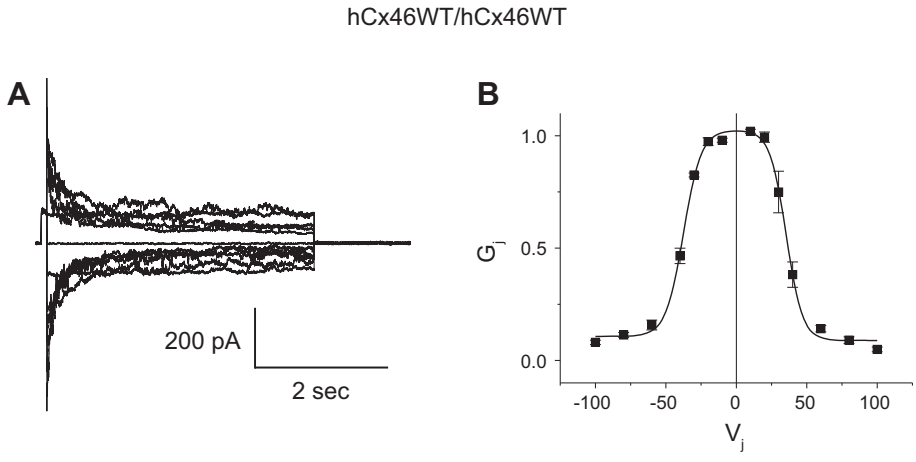


Fig. 4. Properties of human connexin (Cx)46. *A*: macroscopic junctional currents recorded from paired Neuro2a cells expressing human Cx46. *B*: steady-state normalized junctional conductance-junctional voltage ($G_j$-$V_j$) relations for determined from current traces such as those shown in *A*. Solid lines are Boltzmann fits to the data mean data shown by filled squares (error bars represent standard errors of the mean). Fit parameters for $-V_j$: $G_{max}$, 1.01; $G_{min}$, 0.11; $V_0$, −37.5; K, −6.3; for $+V_j$: $G_{max}$, 1.01; $G_{min}$, 0.09; $V_0$, 35.4; K , 5.8; $n$ = 7 cell pairs. Filtering in *A* for display, 500 Hz.

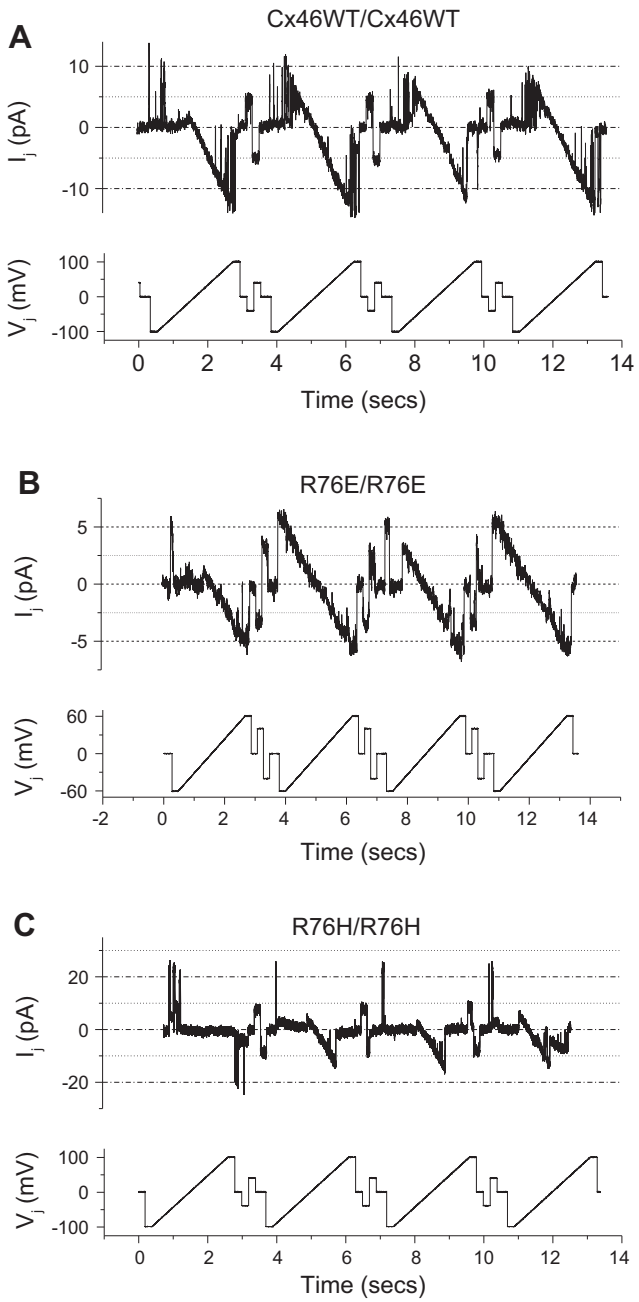


Fig. 5. Recordings of wild-type connexin 46 (Cx46WT) and mutant homotypic cell-cell channels. Unitary conductance transitions of homotypic connexin (Cx)46 (*A*), Cx46R76E (*B*), and Cx46R76H (*C*) channels were determined by applying voltage ramps from −100 to +100 mV (for Cx46 and R76H) or −60 and +60 mV (for R76E) to cell 1 of pairs of Neuro2a cells with only a single active cell-cell channel, measuring the junctional currents ($I_j$) in cell 2, and applying Ohm's law; $n = 12$ for Cx46WT, $n = 4$ for R76H, $n = 2$ for R76E. Filtering for display: *A*, 250 Hz; *B*, 500 Hz; *C*, 500 Hz; *D*, 200 Hz.

(27, 54, 60). Thus, to begin to assess the role of $Arg^{76}$ in the structure of Cx46 and the R76E, R76G, and R76H mutants, we first used ESBRI to evaluate the potential ionic interactions of $Arg^{76}$ and of residues interacting with $Arg^{76}$ by using the MD simulation equilibrated structures. The ionic interactions are defined by at least one carboxyl oxygen and one side-chain nitrogen within a distance of 4.0 Å. As shown in Fig. 7, $Arg^{76}$ forms interprotomeric salt bridges with both $Asp^{43}$ and $Glu^{199}$. $Arg^{76}$ also forms an intraprotomeric salt bridge with $Glu^{48}$. Each of these residues in turn forms other, exclusively intraprotomeric salt bridges; thus, $Arg^{76}$ is a key residue in a ring of intra- and interprotomeric ionic interactions presumably stabilizing the hexameric Cx46 connexon. The R76G substitution completely disrupted the inter- and intraprotomeric interactions, wheras the R76H substitution retained the interaction with $Asp^{43}$. On the other hand, the R76E mutation created a new intraprotomeric salt bridge between $Glu^{76}$ and $Arg^{196}$; however, as for the R76G mutation, both interprotomeric salt bridges were disrupted.

To further quantify the change in the electrostatic interactions caused by mutation during the simulations, linear interaction energy analysis was performed using ten 1-nS data frames from the last 10 nS of simulation trajectories for each system. Because symmetricity is not imposed on the hexamer during the MD simulation, we considered all interactions existing in at least one of the six possible pairs of residues. Table 3 extracted the average and standard deviation of the top five strongest electrostatic interactions with residue 76 from all six possible pairwise interaction in Cx46WT and compared them with the mutants. Data in Table 3 further confirmed that the strongest electrostatic interactions formed by $Arg^{76}$ are interprotomeric salt bridges with $Asp^{43}$ and $Glu^{199}$ as well as intraprotomeric salt bridges with $Glu^{48}$. Loss of a positive charge at position 76 substantially reduced the stabilizing contribution of these interactions, with the effect being largest when a negatively charged residue was inserted, less with a neutral glycine and least with the polar histidine. In addition, there was also a decrease of favorable interaction with the $Ile^{75}$ backbone in all three mutants.

Although an arginine at the corresponding position in Cx32 reduces the stability of the open state in our homology modeling of Cx32 (4), our data for Cx46 suggest that there is no shift in the relationship between open probability and junctional voltage for any of the mutants studied. Thus, the loss of the electrostatic interaction by R75 mutation observed by our simulation does not affect the open probability of the Cx46. This holds both in terms of the demonstration that Cx46 hemichannels containing mutations at $Arg^{76}$ are as efficient at forming functional hemichannels as is wild-type and in terms of the relative symmetry of cell-cell channel currents when our mutants are paired with Cx46WT. However, our studies suggest that the loss of the arginine at position 76 may play a role in the ability of the Cx46 hemichannel to dock with an apposed hemichannel to form a cell-cell channel. It is therefore likely that the loss of inter- and intraprotomeric interactions in the electrostatic cluster has a significant effect on the extracellular domain conformation and dynamics, thus affecting hemichannel docking. To assess the possible allosteric coupling between residue 76 and extracellular domain, we measured the degree of coupled pairwise motion by normalizing the cross-correlation matrix of α-carbon fluctuations over the last 20-ns trajectories (Fig. 8). The zoom-in correlation map indeed showed a strong correlation in the dynamic motion between $Arg^{76}$ and residues at the docking interface extracellular loops. Notably, $Asn^{55}$ and $Gln^{58}$ in the Cx46 extracellular loop E1 corresponded to $Asn^{54}$ and $Gln^{57}$ in Cx26 that were responsible for junctional docking in Cx26 gap junction channels. $Arg^{180}$, $Asn^{188}$, $Thr^{189}$, and $Asp^{191}$ in Cx46 extracellular E2

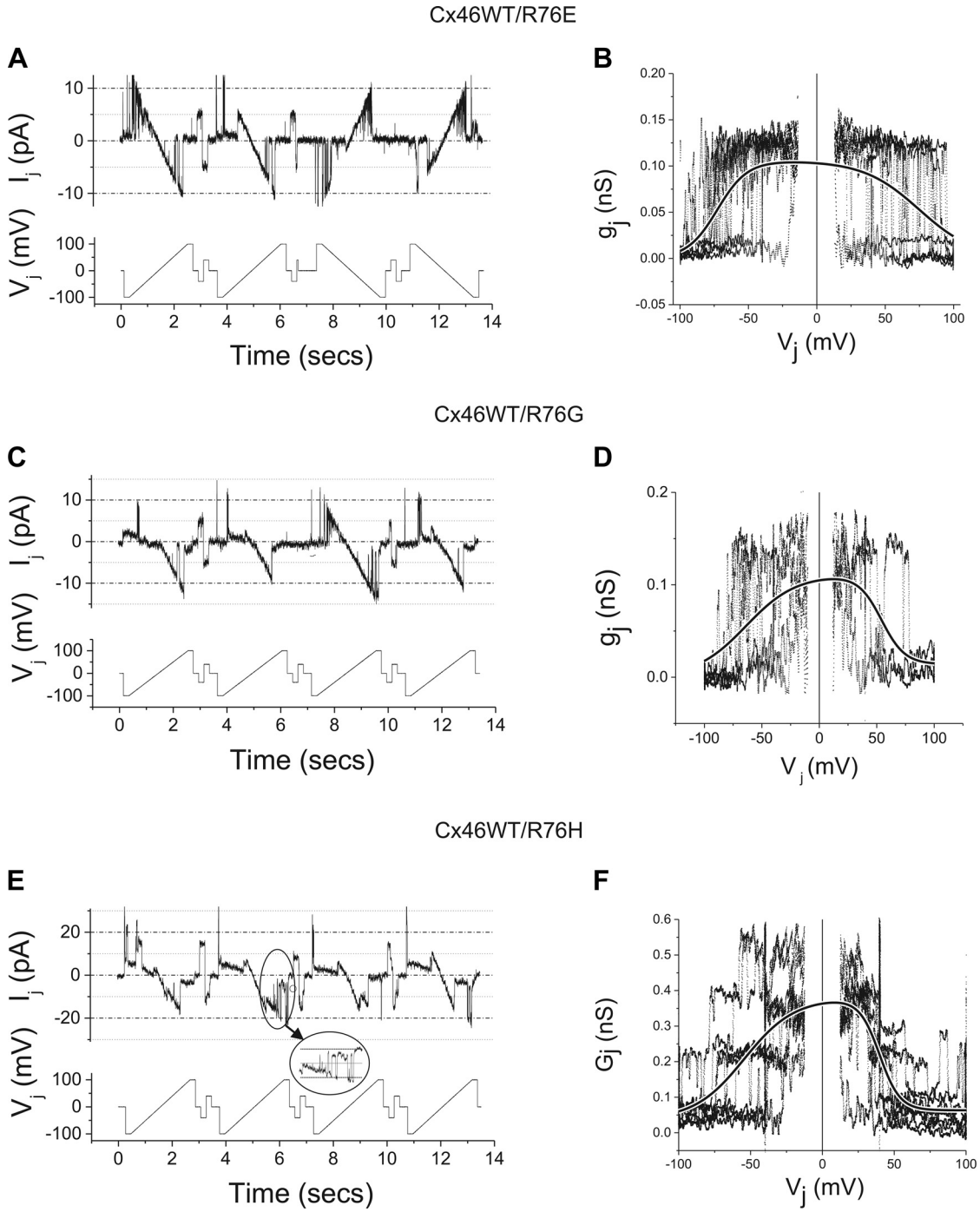


Fig. 6. Cell-cell channel recordings of mutants paired heterotypically with wild-type (WT) connexin (Cx)46. Unitary conductance transitions of heterotypic channels formed by pairing cells expressing Cx46WT with cells expressing mutants Cx46R76E (*A*), Cx46R76G (*C*), and Cx46rR76H (*E*) channels were determined by applying voltage ramps between −100 to +100 mV to cell 1 of pairs of Neuro2a cells with only a single active channel for Cx46/R76E and Cx46/R76G and three active channels for Cx46/R76H and measuring the junctional currents ($I_j$) in cell 2. The relationships between junctional conductance and voltage for each current trace shown in *A*, *C*, and *E* are shown in *B*, *D*, and *F*, respectively. Gray solid lines are Boltzmann fits to the data shown. Although there is some asymmetry of the curves, they are inconsistent with big shifts in the relationship between hemichannel open probability and voltage for the mutants compared with the WT; $n = 3$ for R76E, $n = 3$ for R76G, $n = 3$ for R76H. Filtering for display: *A*, 250 Hz; *C*, 200 Hz; *E*, 200 Hz.

loop corresponded to $Lys^{168}$, $Asn^{176}$, $Thr^{177}$, and $Asp^{179}$ in Cx26 that were responsible for intercellular junctional docking (32). This observation along with experimental results supports our hypothesis that mutation of $Arg^{76}$ may allosterically affect junctional docking. Mutations in $Arg^{75}$ of Cx32 also reduced junctional coupling (4), albeit not to the degree seen for Cx46. We therefore measured the degree of coupled pairwise motion of α-carbon fluctuations over the last 20-nS trajectories for Cx32 and found a similar but somewhat weaker correlation than that which was found for Cx46. That said, a complete understanding of the structural alteration produced by these mutants will require further

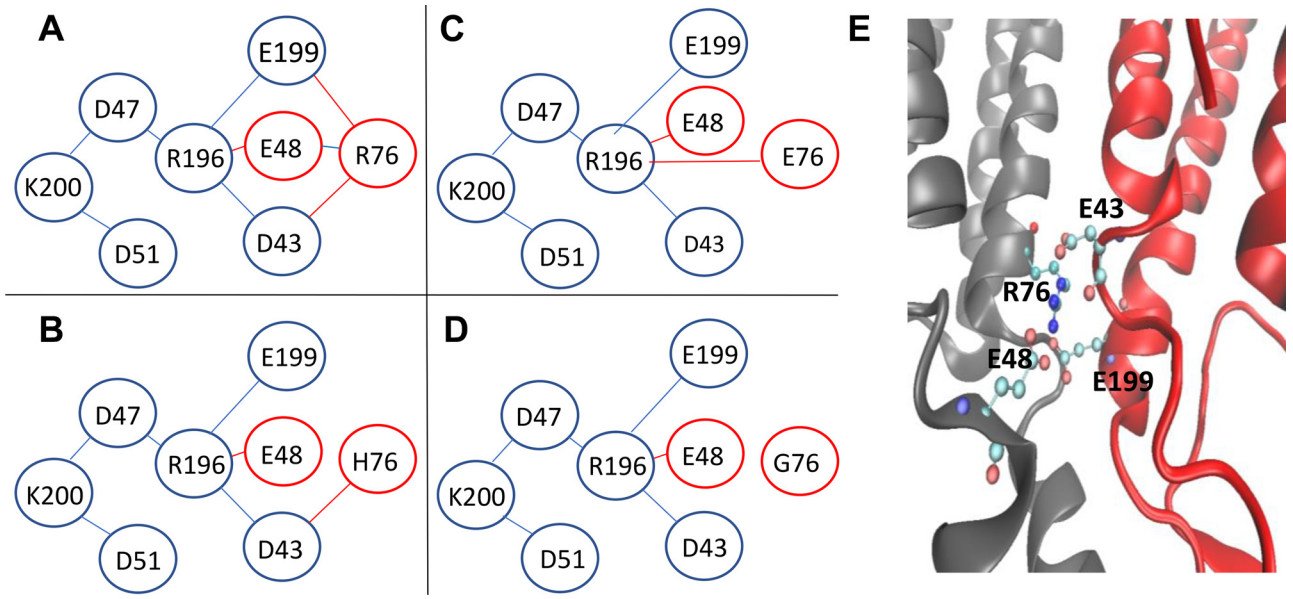


Fig. 7. Predicted salt bridges among residues presumed to form an electrostatic cluster with $Arg^{76}$. Shown are all interactions involving at least one pair of residues within the hexameric structure as described in RESULTS. *A*: prediction for connexin 46 is that $Arg^{76}$ participates in inter- and intraprotomeric salt bridges, thus serving as a lynchpin for the formation of a group of electrostatic interactions throughout the extracellular side of the hexameric structure. *B*: R76E mutation leads to creation of a novel interprotomeric interaction between $Glu^{76}$ and $Arg^{196}$, but there are no predicted intraptotomeric interactions. *C*: introduction of the R76H mutation preserves the interprotomeric interaction with $Asp^{43}$ but disrupts all intraprotomeric interactions. *D*: R76G substitution destroys all inter- and intraprotomeric interactions with $Arg^{76}$. *E*: ribbon diagram showing salt bridges formed with $Arg^{76}$.

investigation on the allosteric regulation of protein-protein interactions using wild-type vs. mutant network analysis across multiple systems (7).

## DISCUSSION

*Mutations in Cx46 at $Arg^{76}$ affect gap junction assembly.* In this communication, we report on our investigations into the properties of the Cx46 wild-type channel and the effects of mutations at codon 76 on the expression and properties of the hemichannel and cell-cell channel formed by Cx46. The formation of gap junction plaques requires several steps. Connexin protein must be expressed, correctly trafficked to and inserted into the cell membrane, and assembled into intercellular gap junction plaques between apposed cells. Musil and colleagues (34) have shown that connexin proteins in gap junction plaques are insoluble in 1% Triton X but that intracellular connexins are not. Here, we have shown that, whereas expression of the wild-type Cx46 leads to the efficient formation of Triton X-insoluble plaques, none of the four mutant forms tested do so to the same extent. Consistent with this finding, none of the four mutants efficiently induces coupling between apposed cells when both express the mutant form of Cx46. Furthermore, this is also true when cells expressing one of the mutant forms of the protein are paired with cells expressing Cx46WT, suggesting that the plaque-forming ability of the WT Cx46 protein cannot functionally rescue the mutants. Nonetheless, our data show that all four mutants of Cx46 are able to produce membrane hemichannels. Although we cannot directly equate levels of dye uptake with equal numbers of active hemichannels because of possible variability in open probability, the presence of measurable dye uptake for all the mutations suggests that each of the mutants is competent

Table 3. *Electrostatic interaction*

| | WT | | R76E | | R76G | | R76H | |
|---|---|---|---|---|---|---|---|---|
| | Mean | SD | Mean | SD | Mean | SD | Mean | SD |
| RES:76 RES:43 (ASP) inter | −83.19 | 1.52 | 28.71 | 4.36 | −1.67 | 0.33 | −2.89 | 1.61 |
| RES:76 RES:48 (GLU) intra | −76.68 | 2.42 | 21.32 | 4.75 | −3.15 | 0.26 | −4.70 | 2.44 |
| RES:76 RES:75 (ILE) intra | −23.35 | 0.33 | −8.25 | 2.46 | −10.75 | 0.17 | −8.91 | 0.25 |
| RES:76 RES:77 (PHE) intra | −10.60 | 0.11 | −11.94 | 0.26 | −11.34 | 0.12 | −11.04 | 0.28 |
| RES:76 RES:199 (GLU) inter | −78.96 | 0.78 | 20.37 | 1.97 | −6.48 | 0.27 | −12.39 | 2.27 |

Means and standard deviation (SD) of each interaction in kcal/mol are calculated from 10 1-nS data frames from the last 10 nS of simulations. Listed are the top 5 strongest interactions with residue (RES) 76 on average from all 6 possible pairwise interactions compared with other mutants. Intra, intraprotomeric; inter, interprotomeric; WT, wild-type.

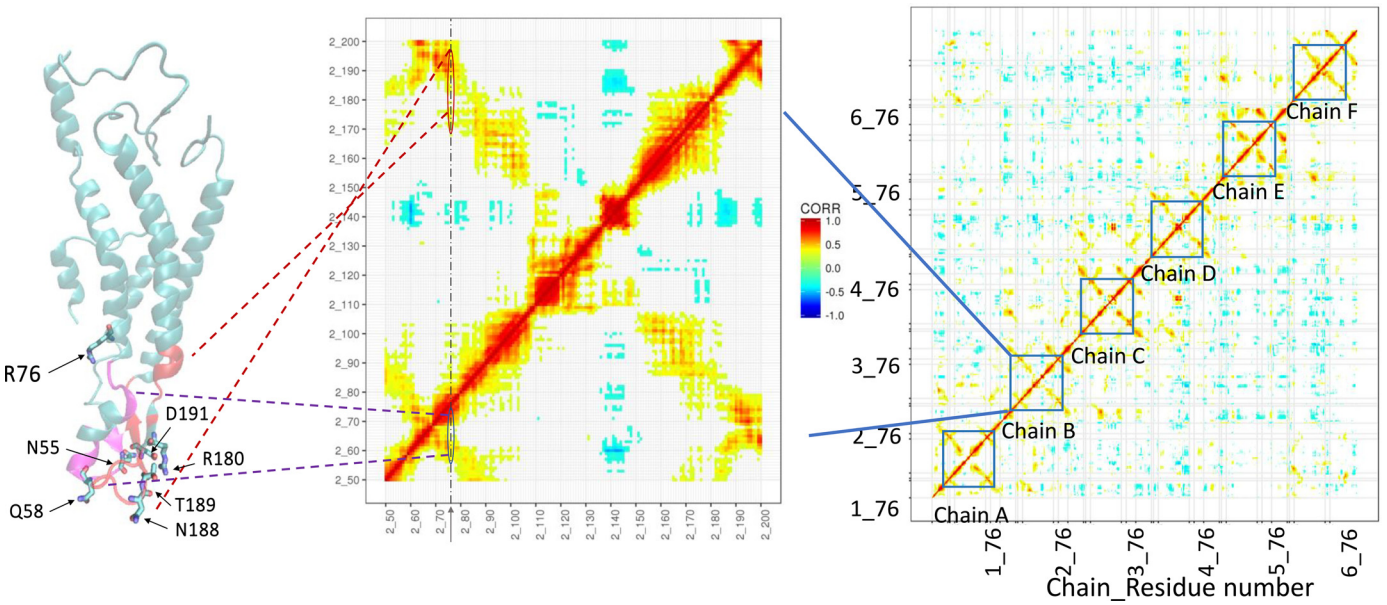


Fig. 8. Correlation analysis of the motion during last 20-ns MD simulation of human connexin (Cx)46. Highly correlated or anticorrelated residue pairs are in red or blue on the correlation map. Regions including residue 76, and the region including extracellular loops is squared for each chain and zoomed in for details. On the protein backbone, residues that have high correlation (>0.5) with R76 are shown in magenta for extracellular loop E1 region (residues 54–63, 69–73), and in red for E2 region (residues 168–177, 179, 182–196). Side chains of residues N55 and Q58 in E1 and R180, N188, T189, and D191 in extracellular loop E2 that correspond to the residues in the Cx26 crystal structure forming intercellular interactions are shown in licorice mode (thick sticks) with atom color code: blue, nitrogen; red, oxygen; and cyan, carbon. Hydrogen atoms are omitted for clarity.

to form a dye-permeable hemichannel. This, in turn, suggests that at least part of the defect in these mutant forms of Cx46 involves the assembly of plaques from membrane-inserted hemichannels, a process that has been described in several different systems (14, 16). As noted above, both the R76G and R76H mutations are associated with inherited cataracts. There is some precedent for mutations in Cx46 associated with inherited cataracts (such as R76G and R76H) to lead to decreased efficiency of gap junction formation with preserved hemichannel forming ability. Schadzek and colleagues (51) have recently shown that, when expressed in oocytes, the N188T mutant efficiently forms hemichannels but shows a significantly reduced number of gap junction plaques. In that case, N188T is located in the second extracellular loop (E2) and is predicted to form hydrogen bonds with residues on the E2 of the apposed connexin monomer, apparently stabilizing the interface between the hemichannels. The failure of the R76E, R76G, and R76H mutants to efficiently form gap junction plaques cannot be attributed to direct involvement of $Arg^{76}$ in intercellular interactions with an apposed connexin. However, we have demonstrated that there is a strong correlation in the dynamic motion between $Arg^{76}$ and residues at the docking interface. This may be due in part to the key role played by $Arg^{76}$ in the electrostatic cluster, which includes residues in or near the docking interface.

*Role of charge at $Arg^{76}$ in the function of connexins.* Prior data from our laboratory have suggested that the charge of the residue at $Arg^{75}$ in Cx32 (the homolog of that of $Arg^{76}$ in Cx46), is critical for Cx32 function. Substitutions at this position had varying effects on the trafficking of Cx32. However, all non-charge-preserving mutations dramatically shifted steady-state conductance voltage relations of the channels produced by heterotypic pairing of these mutants with Cx32 WT, whereas the charge conserving mutations R75K and R75H did not. These data suggest that, at least for Cx32, loss of the positive charge at $Arg^{75}$ stabilizes the closed state relative to the open state of the channel. Furthermore, both the R75K and R75H mutants produced gap junction plaques and induced coupling in both the homotypic configuration and when paired heterotypically with Cx32 WT.

Several studies of mutations at the homologous position of Cx26 have been conducted (9, 11, 40, 44, 48, 49, 58, 62). One of these studies (11), performed in *Xenopus* oocytes, looked at the effects of a number of mutations including the charge-preserving mutation R75K and the charge-changing mutation R75E, and found reduced or absent hemichannel currents and no homotypic coupling for all tested mutants. However, no assessment of morphological gap junction plaques was made. Thus, the relevance of their finding to the role of $Arg^{75/6}$ in gating is difficult to assess, since the lack of any coupling precluded an analysis of gating. Another study (40) used COOH-terminal GFP-tagged forms of Cx26 to look at the effect of the R75E mutation on dye coupling between pairs of cells expressing wild-type or mutant channels. The study demonstrated a substantial reduction, but not elimination, of sulforhodamine dye coupling compared with WT but did not examine the electrical properties of the channel. A caveat to these experiments, however, is that COOH-terminal GFP tagging may have had effects on channel properties. An effect of GFP tagging likely accounts for the discrepancy in reported effects of the introduction of an R75W mutation into Cx26 (62). Oshima and coworkers (40) reported that that cells expressing COOH-terminal-tagged Cx26R75W were coupled at a rate similar to that of wild-type, while Yum and coworkers (62) showed no dye transfer of neurobiotin or lucifer yellow mediated by the untagged R75W protein. These results support

the notion that C-terminal GFP tagging may alter channel behavior in unpredictable ways.

Our data show that heterotypic pairing of the Cx46 R76E, R76G, and R76H mutations produce cell-cell channels exhibiting a relatively symmetric gating response to applied junctional voltage gradients. This suggests that these mutations do not significantly alter the relationship between hemichannel open probability and junctional voltage. This contrasts with our results for Cx32 (4), where loss of the positive charge (or gain of a negative charge) at codon 75 leads to dramatic asymmetries in gating, consistent with either destabilization of the open state or stabilization of the closed state. However, our data for these mutant forms of Cx46 suggest that any changes in stability of the protein induced by them would have to affect the stability of the open and closed states to a similar degree. That said, a complete understanding of the structural and functional alterations produced by these mutants will require detailed atomistic models of both the open and the closed states.

We chose to focus on Cx46 because two different disease-causing mutations in Cx46 have been identified at position 76. As we have shown, the charge-preserving R76K mutation produces no gap junction plaques and no functional coupling. This suggests that our initial hypothesis that preservation of charge at position 76 would be sufficient to preserve incorporation of Cx46 into gap junction plaques turned out to be incorrect. Furthermore, in contrast to our findings with Cx32, preservation of the positive charge at position 76 was not necessary to produce a cell-cell channel with relatively wild-type-like gating properties.

*Conclusion.* Mutations at $Arg^{76}$ (or the homologous position $Arg^{75}$ in Cx26 and Cx32), have been described in a number of genetic disorders, including cataracts (Cx46) (8), hearing loss and/or palmoplantar keratodermia (Cx26) (48), X-linked Charcot Marie Tooth disease (Cx32) (55), and occulodentodigital dysplasia (42) and Hallermann-Streiff syndrome (Cx43). The appearance of pathogenic mutations at this position in a variety of different connexins suggests that this residue likely plays an important role in the function of connexin proteins. Our previous work in Cx32 suggested that the charge at this position, but not necessarily the specific residue, was the most important determinant of whether a particular amino acid change would lead to a pathological state. However, our data here suggest that for Cx46 and possibly for other connexins this is likely not the case, in that the charge-conserving Cx46R76K mutation is completely incompetent to form cell-cell channels. Further study will be required to determine what factors, other than or in addition to charge, are the major determinants of pathogenicity at this position in different connexins.

## ACKNOWLEDGMENTS

Present address of R. Mahmoud: Dept. of Neurology, UMKC School of Medicine–Saint Luke's Hospital, Kansas City, MO (e-mail: rmahmoud@saintlukes.org).

## GRANTS

The computational work was supported by National Science Foundation (NSF) XSEDE research allocation award MCB160119.

## DISCLOSURES

No conflicts of interest, financial or otherwise, are declared by the authors.

## AUTHOR CONTRIBUTIONS

C.K.A., A.P., M.M.F., and Y.L. conceived and designed research; C.K.A., A.P., R.M., H.Z., W.M.B.-S., M.M.F., and Y.L. performed experiments; C.K.A., A.P., M.B., P.C., M.M.F., and Y.L. analyzed data; C.K.A., A.P., M.M.F., and Y.L. interpreted results of experiments; C.K.A., A.P., M.M.F., and Y.L. prepared figures; C.K.A. and Y.L. drafted manuscript; C.K.A., A.P., and Y.L. edited and revised manuscript; C.K.A., A.P., R.M., M.B., H.Z., P.C., W.M.B.-S., M.M.F., and Y.L. approved final version of manuscript.

## REFERENCES

1. **Abrams CK, Freidin M, Bukauskas F, Dobrenis K, Bargiello TA, Verselis VK, Bennett MV, Chen L, Sahenk Z.** Pathogenesis of X-linked Charcot-Marie-Tooth disease: differential effects of two mutations in connexin 32. *J Neurosci* 23: 10548–10558, 2003. doi:10.1523/JNEUROSCI.23-33-10548.2003.
2. **Abrams CK, Freidin MM, Verselis VK, Bennett MV, Bargiello TA.** Functional alterations in gap junction channels formed by mutant forms of connexin 32: evidence for loss of function as a pathogenic mechanism in the X-linked form of Charcot-Marie-Tooth disease. *Brain Res* 900: 9–25, 2001. doi:10.1016/S0006-8993(00)03327-8.
3. **Abrams CK, Goman M, Wong S, Scherer SS, Kleopa KA, Peinado A, Freidin MM.** Loss of Ccoupling distinguishes GJB1 mutations associated with CNS manifestations of CMT1X from those without CNS manifestations. *Sci Rep* 7: 40166, 2017. doi:10.1038/srep40166.
4. **Abrams CK, Islam M, Mahmoud R, Kwon T, Bargiello TA, Freidin MM.** Functional requirement for a highly conserved charged residue at position 75 in the gap junction protein connexin 32. *J Biol Chem* 288: 3609–3619, 2013. doi:10.1074/jbc.M112.392670.
5. **Berthoud VM, Ngezahayo A.** Focus on lens connexins. *BMC Cell Biol* 18, *Suppl* 1: 6, 2017. doi:10.1186/s12860-016-0116-6.
6. **Best RB, Zhu X, Shim J, Lopes PEM, Mittal J, Feig M, Mackerell AD Jr.** Optimization of the additive CHARMM all-atom protein force field targeting improved sampling of the backbone φ, ψ and side-chain χ(1) and χ(2) dihedral angles. *J Chem Theory Comput* 8: 3257–3273, 2012. doi:10.1021/ct300400x.
7. **Botello-Smith WM, Luo Y.** Using current-flow scheme to capture protein allosteric regulation (Preprint). *Biorxiv*. 2018. https://www.biorxiv.org/content/early/2018/02/04/259572.
8. **Burdon KP, Wirth MG, Mackey DA, Russell-Eggitt IM, Craig JE, Elder JE, Dickinson JL, Sale MM.** A novel mutation in the connexin 46 gene causes autosomal dominant congenital cataract with incomplete penetrance. *J Med Genet* 41: e106, 2004. doi:10.1136/jmg.2004.018333.

8a. **Chemical Computing Group.** *Molecular Operating Environment (MOE)*. 1010 Sherbooke St. West, Suite #910. Montreal, QC, Canada, H3A 2R7: Chemical Computing Group, 2018. https://www.chemcomp.com/MOE-Protein_and_Antibody_Modeling.htm.

9. **Chen Y, Deng Y, Bao X, Reuss L, Altenberg GA.** Mechanism of the defect in gap-junctional communication by expression of a connexin 26 mutant associated with dominant deafness. *FASEB J* 19: 1516–1518, 2005. doi:10.1096/fj.04-3491fje.
10. **Costantini S, Colonna G, Facchiano AM.** ESBRI: a web server for evaluating salt bridges in proteins. *Bioinformation* 3: 137–138, 2008. doi:10.6026/97320630003137.
11. **Deng Y, Chen Y, Reuss L, Altenberg GA.** Mutations of connexin 26 at position 75 and dominant deafness: essential role of arginine for the generation of functional gap-junctional channels. *Hear Res* 220: 87–94, 2006. doi:10.1016/j.heares.2006.07.004.
12. **Devi RR, Reena C, Vijayalakshmi P.** Novel mutations in GJA3 associated with autosomal dominant congenital cataract in the Indian population. *Mol Vis* 11: 846–852, 2005.
13. **Doble BW, Dang X, Ping P, Fandrich RR, Nickel BE, Jin Y, Cattini PA, Kardami E.** Phosphorylation of serine 262 in the gap junction protein connexin-43 regulates DNA synthesis in cell-cell contact forming cardiomyocytes. *J Cell Sci* 117: 507–514, 2004. doi:10.1242/jcs.00889.
14. **Flores CE, Nannapaneni S, Davidson KG, Yasumura T, Bennett MV, Rash JE, Pereda AE.** Trafficking of gap junction channels at a vertebrate electrical synapse in vivo. *Proc Natl Acad Sci USA* 109: E573–E582, 2012. [Erratum in *Proc Natl Acad Sci USA* 110: 18735, 2013.] doi:10.1073/pnas.1121557109.
15. **Freidin M, Asche S, Bargiello TA, Bennett MV, Abrams CK.** Connexin 32 increases the proliferative response of Schwann cells to neuregulin-1 (Nrg1). *Proc Natl Acad Sci USA* 106: 3567–3572, 2009. doi:10.1073/pnas.0813413106.

16. **Gaietta G, Deerinck TJ, Adams SR, Bouwer J, Tour O, Laird DW, Sosinsky GE, Tsien RY, Ellisman MH.** Multicolor and electron microscopic imaging of connexin trafficking. *Science* 296: 503–507, 2002. doi:10.1126/science.1068793.
17. **Giepmans BN, Moolenaar WH.** The gap junction protein connexin43 interacts with the second PDZ domain of the zona occludens-1 protein. *Curr Biol* 8: 931–934, 1998. doi:10.1016/S0960-9822(07)00375-2.
18. **Glykos NM.** Software news and updates. Carma: a molecular dynamics analysis program. *J Comput Chem* 27: 1765–1768, 2006. doi:10.1002/jcc.20482.
19. **Hopperstad MG, Srinivas M, Spray DC.** Properties of gap junction channels formed by Cx46 alone and in combination with Cx50. *Biophys J* 79: 1954–1966, 2000. doi:10.1016/S0006-3495(00)76444-7.
20. **Jo S, Kim T, Iyer VG, Im W.** CHARMM-GUI: a web-based graphical user interface for CHARMM. *J Comput Chem* 29: 1859–1865, 2008. doi:10.1002/jcc.20945.
21. **Jorgensen WL, Chandrasekhar J, Madura JD, Impey RW, Klein MLK.** Comparison of simple potential functions for simulating liquid water. *J Chem Phys* 79: 926–935, 1983. doi:10.1063/1.445869.
22. **Kausalya PJ, Reichert M, Hunziker W.** Connexin45 directly binds to ZO-1 and localizes to the tight junction region in epithelial MDCK cells. *FEBS Lett* 505: 92–96, 2001. doi:10.1016/S0014-5793(01)02786-7.
23. **Klauda JB, Venable RM, Freites JA, O'Connor JW, Tobias DJ, Mondragon-Ramirez C, Vorobyov I, MacKerell AD Jr, Pastor RW.** Update of the CHARMM all-atom additive force field for lipids: validation on six lipid types. *J Phys Chem B* 114: 7830–7843, 2010. doi:10.1021/jp101759q.
25. **Kwon T, Harris AL, Rossi A, Bargiello TA.** Molecular dynamics simulations of the Cx26 hemichannel: evaluation of structural models with Brownian dynamics. *J Gen Physiol* 138: 475–493, 2011. doi:10.1085/jgp.201110679.
27. **Kwon T, Roux B, Jo S, Klauda JB, Harris AL, Bargiello TA.** Molecular dynamics simulations of the Cx26 hemichannel: insights into voltage-dependent loop-gating. *Biophys J* 102: 1341–1351, 2012. doi:10.1016/j.bpj.2012.02.009.
28. **Li X, Ionescu AV, Lynn BD, Lu S, Kamasawa N, Morita M, Davidson KG, Yasumura T, Rash JE, Nagy JI.** Connexin47, connexin29 and connexin32 co-expression in oligodendrocytes and Cx47 association with zonula occludens-1 (ZO-1) in mouse brain. *Neuroscience* 126: 611–630, 2004. doi:10.1016/j.neuroscience.2004.03.063.
29. **Li X, Olson C, Lu S, Kamasawa N, Yasumura T, Rash JE, Nagy JI.** Neuronal connexin36 association with zonula occludens-1 protein (ZO-1) in mouse brain and interaction with the first PDZ domain of ZO-1. *Eur J Neurosci* 19: 2132–2146, 2004. doi:10.1111/j.0953-816X.2004.03283.x.
30. **Lin JH, Yang J, Liu S, Takano T, Wang X, Gao Q, Willecke K, Nedergaard M.** Connexin mediates gap junction-independent resistance to cellular injury. *J Neurosci* 23: 430–441, 2003. doi:10.1523/JNEUROSCI.23-02-00430.2003.
31. **Luo Y, Rossi AR, Harris AL.** Computational studies of molecular permeation through connexin26 channels. *Biophys J* 110: 584–599, 2016. doi:10.1016/j.bpj.2015.11.3528.
32. **Maeda S, Nakagawa S, Suga M, Yamashita E, Oshima A, Fujiyoshi Y, Tsukihara T.** Structure of the connexin 26 gap junction channel at 3.5 A resolution. *Nature* 458: 597–602, 2009. doi:10.1038/nature07869.
33. **Moorby C, Patel M.** Dual functions for connexins: Cx43 regulates growth independently of gap junction formation. *Exp Cell Res* 271: 238–248, 2001. doi:10.1006/excr.2001.5357.
34. **Musil LS, Goodenough DA.** Biochemical analysis of connexin43 intracellular transport, phosphorylation, and assembly into gap junctional plaques. *J Cell Biol* 115: 1357–1374, 1991. doi:10.1083/jcb.115.5.1357.
35. **Nielsen PA, Baruch A, Shestopalov VI, Giepmans BN, Dunia I, Benedetti EL, Kumar NM.** Lens connexins alpha3Cx46 and alpha8Cx50 interact with zonula occludens protein-1 (ZO-1). *Mol Biol Cell* 14: 2470–2481, 2003. doi:10.1091/mbc.e02-10-0637.
36. **Oguro K, Jover T, Tanaka H, Lin Y, Kojima T, Oguro N, Grooms SY, Bennett MV, Zukin RS.** Global ischemia-induced increases in the gap junctional proteins connexin 32 (Cx32) and Cx36 in hippocampus and enhanced vulnerability of Cx32 knock-out mice. *J Neurosci* 21: 7534–7542, 2001. doi:10.1523/JNEUROSCI.21-19-07534.2001.
37. **Omori Y, Yamasaki H.** Mutated connexin43 proteins inhibit rat glioma cell growth suppression mediated by wild-type connexin43 in a dominant-negative manner. *Int J Cancer* 78: 446–453, 1998. doi:10.1002/(SICI)1097-0215(19981109)78:4<446::AID-IJC10>3.0.CO;2-4.
38. **Orthmann-Murphy JL, Enriquez AD, Abrams CK, Scherer SS.** Loss-of-function GJA12/connexin47 mutations cause Pelizaeus-Merzbacher-like disease. *Mol Cell Neurosci* 34: 629–641, 2007. doi:10.1016/j.mcn.2007.01.010.
39. **Orthmann-Murphy JL, Freidin M, Fischer E, Scherer SS, Abrams CK.** Two distinct heterotypic channels mediate gap junction coupling between astrocyte and oligodendrocyte connexins. *J Neurosci* 27: 13949–13957, 2007. doi:10.1523/JNEUROSCI.3395-07.2007.
40. **Oshima A, Doi T, Mitsuoka K, Maeda S, Fujiyoshi Y.** Roles of Met-34, Cys-64, and Arg-75 in the assembly of human connexin 26. Implication for key amino acid residues for channel formation and function. *J Biol Chem* 278: 1807–1816, 2003. doi:10.1074/jbc.M207713200.
41. **Paul DL, Ebihara L, Takemoto LJ, Swenson KI, Goodenough DA.** Connexin46, a novel lens gap junction protein, induces voltage-gated currents in nonjunctional plasma membrane of *Xenopus* oocytes. *J Cell Biol* 115: 1077–1089, 1991. doi:10.1083/jcb.115.4.1077.
42. **Paznekas WA, Boyadjiev SA, Shapiro RE, Daniels O, Wollnik B, Keegan CE, Innis JW, Dinulos MB, Christian C, Hannibal MC, Jabs EW.** Connexin 43 (GJA1) mutations cause the pleiotropic phenotype of oculodentodigital dysplasia. *Am J Hum Genet* 72: 408–418, 2003. doi:10.1086/346090.
43. **Penes MC, Li X, Nagy JI.** Expression of zonula occludens-1 (ZO-1) and the transcription factor ZO-1-associated nucleic acid-binding protein (ZONAB)-MsY3 in glial cells and colocalization at oligodendrocyte and astrocyte gap junctions in mouse brain. *Eur J Neurosci* 22: 404–418, 2005. doi:10.1111/j.1460-9568.2005.04225.x.
44. **Piazza V, Beltramello M, Menniti M, Colao E, Malatesta P, Argento R, Chiarella G, Gallo LV, Catalano M, Perrotti N, Mammano F, Cassandro E.** Functional analysis of R75Q mutation in the gene coding for Connexin 26 identified in a family with nonsyndromic hearing loss. *Clin Genet* 68: 161–166, 2005. doi:10.1111/j.1399-0004.2005.00468.x.
45. **Qin H, Shao Q, Curtis H, Galipeau J, Belliveau DJ, Wang T, Alaoui-Jamali MA, Laird DW.** Retroviral delivery of connexin genes to human breast tumor cells inhibits in vivo tumor growth by a mechanism that is independent of significant gap junctional intercellular communication. *J Biol Chem* 277: 29132–29138, 2002. doi:10.1074/jbc.M200797200.
46. **Ren Q, Riquelme MA, Xu J, Yan X, Nicholson BJ, Gu S, Jiang JX.** Cataract-causing mutation of human connexin 46 impairs gap junction, but increases hemichannel function and cell death. *PLoS One* 8: e74732, 2013. doi:10.1371/journal.pone.0074732.
48. **Richard G, White TW, Smith LE, Bailey RA, Compton JG, Paul DL, Bale SJ.** Functional defects of Cx26 resulting from a heterozygous missense mutation in a family with dominant deaf-mutism and palmoplantar keratoderma. *Hum Genet* 103: 393–399, 1998. doi:10.1007/s004390050839.
49. **Rouan F, White TW, Brown N, Taylor AM, Lucke TW, Paul DL, Munro CS, Uitto J, Hodgins MB, Richard G.** trans-dominant inhibition of connexin-43 by mutant connexin-26: implications for dominant connexin disorders affecting epidermal differentiation. *J Cell Sci* 114: 2105–2113, 2001.
50. **Sakai R, Elfgang C, Vogel R, Willecke K, Weingart R.** The electrical behaviour of rat connexin46 gap junction channels expressed in transfected HeLa cells. *Pflugers Arch* 446: 714–727, 2003. doi:10.1007/s00424-003-1129-5.
51. **Schadzek P, Schlingmann B, Schaarschmidt F, Lindner J, Koval M, Heisterkamp A, Preller M, Ngezahayo A.** The cataract related mutation N188T in human connexin46 (hCx46) revealed a critical role for residue N188 in the docking process of gap junction channels. *Biochim Biophys Acta* 1858: 57–66, 2016. doi:10.1016/j.bbamem.2015.10.001.
52. **Söhl G, Willecke K.** Gap junctions and the connexin protein family. *Cardiovasc Res* 62: 228–232, 2004. doi:10.1016/j.cardiores.2003.11.013.
53. **Stout C, Goodenough DA, Paul DL.** Connexins: functions without junctions. *Curr Opin Cell Biol* 16: 507–512, 2004. doi:10.1016/j.ceb.2004.07.014.
54. **Tang Q, Dowd TL, Verselis VK, Bargiello TA.** Conformational changes in a pore-forming region underlie voltage-dependent "loop gating" of an unapposed connexin hemichannel. *J Gen Physiol* 133: 555–570, 2009. doi:10.1085/jgp.200910207.
55. **Taylor RA, Simon EM, Marks HG, Scherer SS.** The CNS phenotype of X-linked Charcot-Marie-Tooth disease: more than a peripheral problem. *Neurology* 61: 1475–1478, 2003. doi:10.1212/01.WNL.0000095960.48964.25.
56. **Tong JJ, Sohn BC, Lam A, Walters DE, Vertel BM, Ebihara L.** Properties of two cataract-associated mutations located in the $NH_2$ terminus of connexin 46. *Am J Physiol Cell Physiol* 304: C823–C832, 2013. doi:10.1152/ajpcell.00344.2012.

57. **Trexler EB, Bukauskas FF, Kronengold J, Bargiello TA, Verselis VK.** The first extracellular loop domain is a major determinant of charge selectivity in connexin46 channels. *Biophys J* 79: 3036–3051, 2000. doi:10.1016/S0006-3495(00)76539-8.
58. **Uyguner O, Tukel T, Baykal C, Eris H, Emiroglu M, Hafiz G, Ghanbari A, Baserer N, Yuksel-Apak M, Wollnik B.** The novel R75Q mutation in the GJB2 gene causes autosomal dominant hearing loss and palmoplantar keratoderma in a Turkish family. *Clin Genet* 62: 306–309, 2002. doi:10.1034/j.1399-0004.2002.620409.x.
59. **VanSlyke JK, Deschenes SM, Musil LS.** Intracellular transport, assembly, and degradation of wild-type and disease-linked mutant gap junction proteins. *Mol Biol Cell* 11: 1933–1946, 2000. doi:10.1091/mbc.11.6.1933.
60. **Verselis VK, Trelles MP, Rubinos C, Bargiello TA, Srinivas M.** Loop gating of connexin hemichannels involves movement of pore-lining residues in the first extracellular loop domain. *J Biol Chem* 284: 4484–4493, 2009. doi:10.1074/jbc.M807430200.
61. **White TW, Bruzzone R, Goodenough DA, Paul DL.** Mouse Cx50, a functional member of the connexin family of gap junction proteins, is the lens fiber protein MP70. *Mol Biol Cell* 3: 711–720, 1992. doi:10.1091/mbc.3.7.711.
62. **Yum SW, Zhang J, Scherer SS.** Dominant connexin26 mutants associated with human hearing loss have trans-dominant effects on connexin30. *Neurobiol Dis* 38: 226–236, 2010. doi:10.1016/j.nbd.2010.01.010.